

Structure and Corrosion Resistance of $\text{Ca}_{50}\text{Mg}_{20}\text{Cu}_{30}$ Bulk Metallic Glasses

Rafał Babilas, Katarzyna Cesarz-Andraczke, Dorota Babilas, and Wojciech Simka

(Submitted June 4, 2014; in revised form October 3, 2014; published online November 15, 2014)

The ternary $\text{Ca}_{50}\text{Mg}_{20}\text{Cu}_{30}$ bulk metallic glass with thickness of 1 mm and width of 10 mm was successfully fabricated by conventional copper-mold casting method. The structural characterization of the alloy in the “as-cast” and after-annealing states was carried out using x-ray diffraction method. The corrosion behaviors of the glassy and crystalline samples were studied by electrochemical measurements and immersion tests in a 5% NaCl solution at room temperature. The amorphous alloy showed higher corrosion resistance than crystalline samples. The post-test analyses were conducted by scanning electron microscopy and energy-dispersive x-ray spectroscopy to examine the damage and chemical composition of the investigated surfaces.

Keywords bulk metallic glasses, Ca-based alloys, corrosion resistance, thermal analysis

1. Introduction

Calcium-based bulk metallic glasses are a new class of engineering materials with low density ($\sim 2.0 \text{ g/cm}^3$), low Young's modulus ($\sim 20\text{--}35 \text{ GPa}$), low glass-transition temperature ($\sim 80\text{--}150 \text{ }^\circ\text{C}$), and high glass-forming ability (GFA). The first Ca-based amorphous alloys of the following chemical compositions: Ca-Mg-Cu, Ca-Mg-Zn, and Ca-Mg-Ag-Cu have been obtained in 2002 (Ref 1-3). High GFA determined by supercooled liquid region (up to 70 K) allows obtaining glassy alloy with a maximum diameter of 15 mm produced by copper-mold casting (Ref 4). However, only a few studies describe the metallic materials properties (Ref 5).

Calcium is an extremely reactive metal and spontaneously reacts with water generating hydrogen. Compared to the other metals, calcium and most of its compounds have low toxicity. This is not surprising given the very high natural abundance of calcium compounds in the environment and in living organisms. Crystalline calcium-based alloys are oxidized in air within a few days, while a large number of Ca-based amorphous alloys (i.e., Ca-Mg-Cu, Ca-Mg-Al, etc.) have satisfactory oxidation resistance and maintain shiny surfaces for a long time after casting (Ref 6, 7).

Morrison et al. (Ref 8) performed the electrochemical corrosion studies of Ca-Mg-Cu, Ca-Mg-Zn, and Ca-Mg-Zn-Cu bulk metallic glasses in a 0.05 M Na_2SO_4 electrolyte. Both the Ca-Mg-Zn-Cu and Ca-Mg-Zn alloys were found to be suscep-

tible to the pitting corrosion; however, Ca-Mg-Cu metallic glass showed only localized corrosion. Corrosion resistance studies of Ca-based metallic glasses are necessary to explore the limiting factors for their practical application.

Senkov et al. (Ref 9) carried out immersion corrosion studies of Ca-Mg-Zn and Ca-Mg-Cu amorphous alloys. The examined materials demonstrated poor corrosion resistance. After 700 h of exposure in distilled water, the Ca-Mg-Cu alloy was completely decomposed into a mixture of compounds, consisting of two major phases: Cu_2O and $\text{Ca}(\text{OH})_2$, while $\text{Ca}_{65}\text{Mg}_{15}\text{Zn}_{20}$ amorphous alloy decomposed into three primary phases: $\text{Ca}(\text{OH})_2$, Ca_3Zn , and $\text{Ca}[\text{Zn}(\text{OH})_3] \cdot 2\text{H}_2\text{O}$.

The authors of the paper succeeded in the preparation of Ca-based metallic glasses in bulk samples, which are potential candidates for constructional materials. This paper verifies the structure and corrosion behavior of $\text{Ca}_{50}\text{Mg}_{20}\text{Cu}_{30}$ alloy in the “as-cast” state and after annealing in comparison with pure Mg and Cu in NaCl solution.

2. Materials and Methods

The studies were performed on $\text{Ca}_{50}\text{Mg}_{20}\text{Cu}_{30}$ (at.%) bulk metallic glasses, pure magnesium, and copper plates ($1 \times 10 \times 10 \text{ mm}$). The master alloys were prepared by mixing and induction melting of pure elements: Ca (99.9%), Mg (99.9%), and Cu (99.99%) in a protective atmosphere. The prepared alloys in the form of ingots were induction remelted in a quartz crucible and then injected into the copper mold by the pressure casting method to fabricate 1-mm-thick plates (Ref 10-13).

To study the crystallization process, the samples in the “as-cast” state were annealed in the temperatures ranging from 373 to 573 K. The investigated plates were annealed in a Thermolyne 6020C electric chamber furnace under protective argon atmosphere. The annealing time was constant and equal to 1 h.

The structures of the samples in the “as-cast” state and after annealing were determined by x-ray diffraction (XRD) in the reflection mode using a Seifert-FPM XRD 7 diffractometer with $\text{Co K}\alpha$ radiation source (wavelength = 0.17902 nm). The

Rafał Babilas and **Katarzyna Cesarz-Andraczke**, Institute of Engineering Materials and Biomaterials, Silesian University of Technology, Konarskiego Street 18a, 44-100 Gliwice, Poland; and **Dorota Babilas** and **Wojciech Simka**, Department of Inorganic, Analytical Chemistry and Electrochemistry, Silesian University of Technology, B. Krzywoustego Street 6, 44-100 Gliwice, Poland. Contact e-mail: rafal.babilas@polsl.pl.

diffraction patterns were recorded by “step-scanning” method in the range from 30° to 90° of 2θ angle.

For the analysis of XRD patterns in the “as-cast” state, the experimental diffraction peak has been reproduced by means of Lorentz function approximation. The x-ray broad diffraction halo was plotted in the scattering vector (Q) that ranged between 18 and 34 nm⁻¹:

$$Q = \frac{4\pi \sin\theta}{\lambda}, \quad (\text{Eq 1})$$

where 2θ is the angle between the incident and the scattered beams; and λ is the wavelength.

The scattering vector is defined as the difference between the wave vectors, each with the magnitude of 2π/λ, in the directions of the incident and scattered beams, respectively. Analysis of the position and the width of the x-ray amorphous halo may provide some information on the nearest interatomic spacing in the amorphous structure. The position of an x-ray halo maximum is known to be directly related with the average radius of the first coordination shell (Ref 14).

The glass-transition temperature (T_g) and crystallization analysis associated with the onset (T_x), and the peak crystallization (T_p) of the studied samples were determined by the differential scanning calorimetry (DSC) using a DuPont 910 device in the temperatures ranging from 350 to 500 K and a constant heating rate of 20 K/min under argon atmosphere.

Thermal properties of the studied master alloy were tested by a differential thermal analysis (DTA) using a TA-1 Mettler thermal analyzer in the temperatures ranging from 500 to 800 K at a constant heating rate of 6 K/s under argon atmosphere.

The fracture and surface morphologies of the glassy samples before and after corrosion tests were analyzed using a scanning electron microscope (SEM) Supra 35 Carl Zeiss with the energy-dispersive x-ray spectroscopy (EDS) EDAX.

The corrosion behaviors of the bulk glassy alloy in the “as-cast” state and after annealing were studied by immersion tests and electrochemical measurements. The immersion tests in a 5% NaCl solution at room temperature were conducted to calculate the corrosion rate (V_{CORR}) and to determine an amount of evolved hydrogen of Ca₅₀Cu₃₀Mg₂₀ bulk metallic glass. The immersion time was 70 min. Based on the recommended experimental set up described in (Ref 15-18), the amount of evolved hydrogen was measured using a gas burette. The Ca₅₀Cu₃₀Mg₂₀ sample was put in a beaker with a 5% NaCl solution. A funnel was placed over the sample, which ensured the collection of hydrogen from the specimen surface. Burette was mounted over the funnel and filled with the solution.

The electrochemical investigations of the studied alloy (in the “as-cast” and after heat treatment at 573 K for 1 h) and reference samples (pure Mg and Cu) were performed in a standard thermostated electrolysis cell. The measurements were conducted in a 5% NaCl solution at room temperature. Following materials served as electrodes: the sample—working electrode; a saturated calomel electrode (SCE) with a Haber-Luggin capillary—reference electrode; and a platinum mesh—counter electrode. The measurements were conducted using a PARSTAT 4000 potentiostat and Versa Studio software. The following procedures were carried out to evaluate the corrosion resistance of the studied samples: (a) recording of the open-circuit potential (E_{OCP}) variation, (b) evaluation of potentiodynamic polarization curves in the potential range $E_{\text{OCP}} - 250$ mV to $E_{\text{OCP}} + 250$ mV ($dE/dt = 1$ mV/s), along with short-range of E_{OCP} from 20 mV to $E_{\text{OCP}} + 20$ mV polarization scan

to determine corrosion potential (E_{CORR}), corrosion current density (i_{CORR}), and polarization resistance (R_p) according to Stern-Geary method:

$$i_{\text{CORR}} = \frac{\beta_a \beta_c}{2.3(|\beta_a| + |\beta_c|) R_p} = \frac{B}{R_p}, \quad (\text{Eq 2})$$

where β_a is anodic and β_c is cathodic Tafel slopes calculated from the Tafel extrapolation.

All samples were measured from a near-steady-state corrosion potential, and after a period of open-circuit potential stabilization, the E_{OCP} was monitored for 60 min for each sample.

3. Results and Discussion

The XRD pattern of the Ca₅₀Mg₂₀Cu₃₀ alloy in the “as-cast” state is presented in Fig. 1(a). The diffraction pattern of the studied sample showed a broad diffraction halo indicating the formation of an amorphous structure. Figure 1(b) shows the intensity of the x-ray scattering versus $Q = 4\pi \sin\theta/\lambda$ for the examined amorphous alloy, where 2θ is the angle of deviation of the diffracted beam. It can be seen that the value of Q corresponding to the position of the scatter intensity peak appears at about 23.6 nm⁻¹.

The broad diffraction peak shows the asymmetric profile, which could be deconvoluted into two Lorentz distribution functions. The peaks of fitted functions have values of 23.2 and 26.5 nm⁻¹. Such behavior is the evidence of topologic

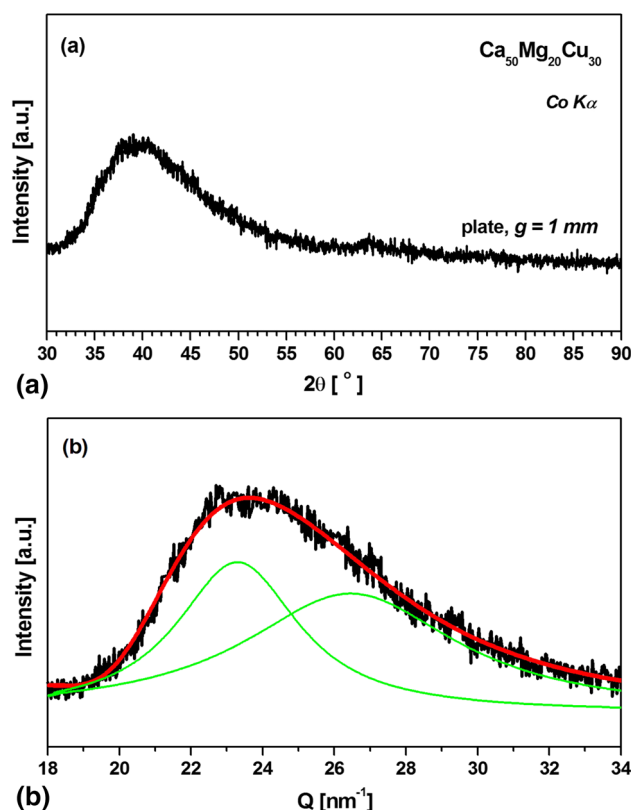


Fig. 1 X-ray diffraction pattern (a) and fitted functions of Lorentz distribution (b) of the Ca₅₀Mg₂₀Cu₃₀ alloy plate

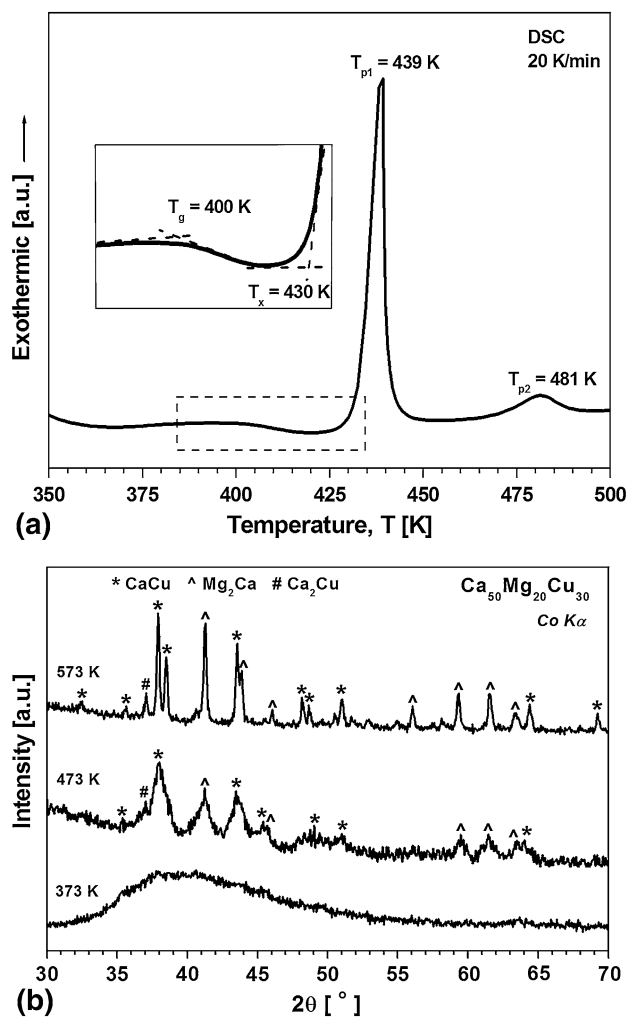


Fig. 2 DSC curves (a) and x-ray diffraction patterns after annealing (b) of the examined metallic glass

ordering, which is supposed to be caused by atomic rearrangement due to decrease of free volume. Besides, the two components of the Lorentz function indicated the coexistence of two different neighbor-shell surroundings of the Ca atoms, which are commonly called as clusters.

These clusters may contain various volume fractions of Ca, Mg, and Cu elements. Similar decomposition of the amorphous structure was described in (Ref 19) for the bulk glassy $\text{Ca}_{60}\text{Mg}_{20}\text{Cu}_{20}$ alloy. The neutron and XRD pair correlation functions were fitted with a series of symmetric peaks to obtain coordination numbers and interatomic distances. Those authors state that there are contacts between the solute atoms (Cu and Mg) and the Cu-Mg and Cu-Ca distances are consistent with the sum of covalent radii. Such more complex amorphous structures consisting of at least two kinds of atomic clusters were formed simultaneously during the rapid solidification process.

The DSC curves obtained from the “as-cast” sample during continuous heating at a rate of 20 K/min are shown in Fig. 2(a). The exothermic effects corresponding to the crystallization process of glassy material and the endothermic reaction corresponding to the glass-transition are clearly observed. The effects also exhibit the sequence of the glass-transition (T_g), the onset (T_x), and peak (T_p) crystallization temperatures. More-

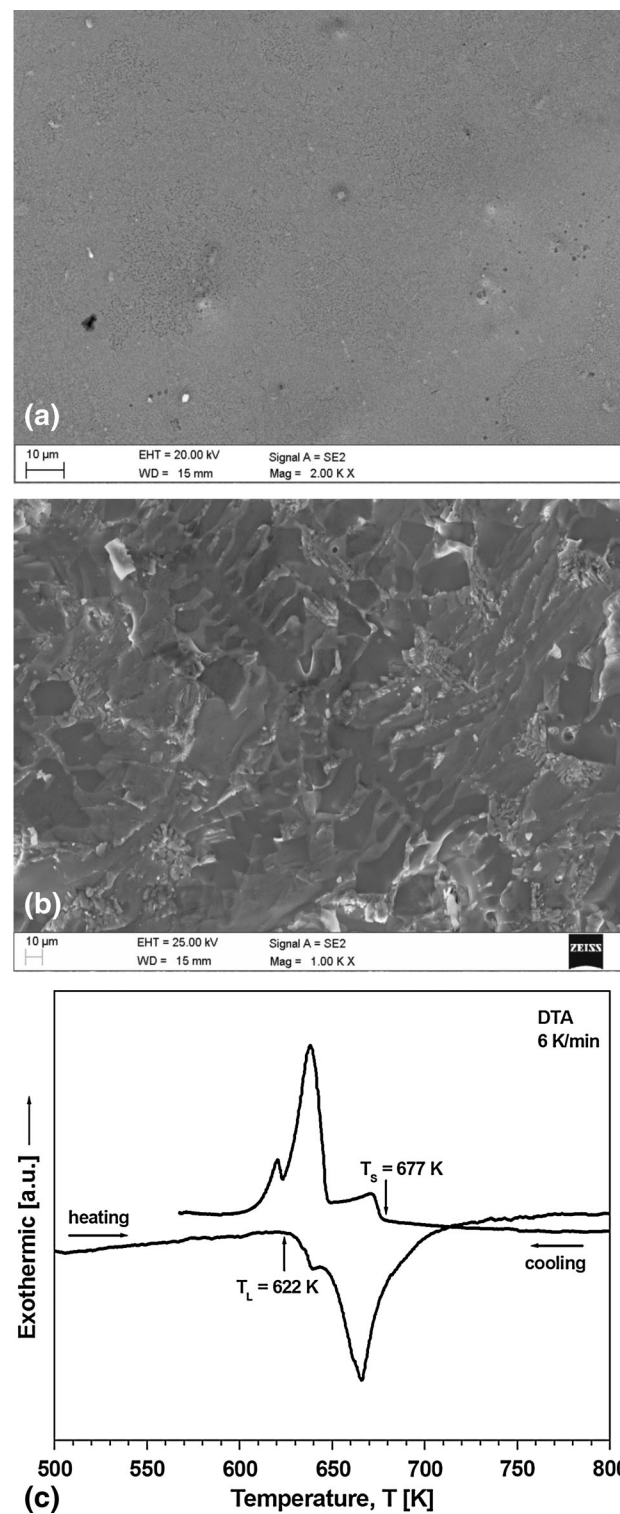


Fig. 3 SEM micrographs of surfaces (a), fracture (b), and morphology and DTA curves (c) of $\text{Ca}_{50}\text{Mg}_{20}\text{Cu}_{30}$ master alloy in the as-cast state

over, two exothermic peaks prove that the two-stage crystallization took place. The onset crystallization temperature reached 430 K. Similarly, the first peak of crystallization temperature was equal to 439 K, and the temperature of the second crystallization stage was 481 K. The DSC analysis allowed the determination of the glass-transition temperature of

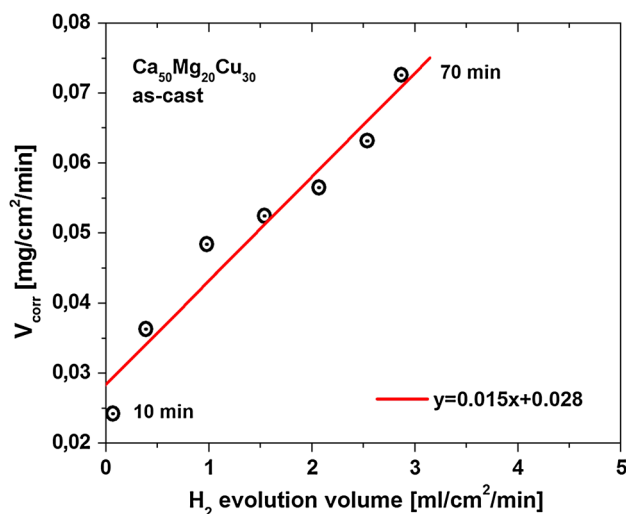


Fig. 4 The independent measurements of weight loss and hydrogen evolution rate for 70 min immersion tests of $\text{Ca}_{50}\text{Mg}_{20}\text{Cu}_{30}$ alloy in the as-cast state in a 5% NaCl solution at room temperature

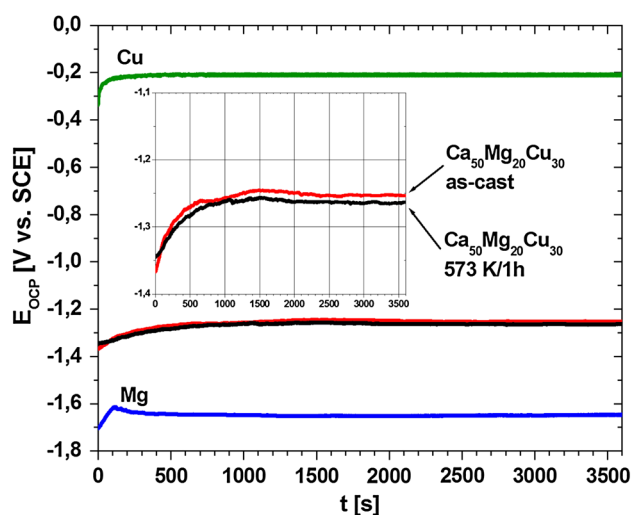


Fig. 5 The variation of the E_{OCP} with time for the studied samples in a 5% NaCl solution at room temperature

the investigated sample, which was 400 K. The temperature interval of the supercooled liquid region (ΔT_x) defined by the difference between T_g and T_x , reached a value of 30 K. The obtained DSC results are in agreement with the research conducted by Senkov et al. (Ref 2).

Figure 2(b) shows the XRD patterns obtained for the tested metallic glasses after annealing at 373, 473, and 573 K for 1 h. At 373 K, no sharp peaks, typical for crystalline materials, were observed. The diffraction pattern exhibits only very broad features characteristic for amorphous materials. The XRD patterns of the samples after annealing at 473 K contain diffraction lines identified according to (Ref 20) as corresponding to the crystalline hexagonal Mg_2Ca and orthorhombic CaCu , Ca_2Cu phases. At 573 K, the intensities of diffraction lines increase, which indicates the growth of CaCu crystallites and Mg_2Ca from the amorphous matrix. These results are consistent with the calorimetric studies, where at 430 K, the onset of crystallization process was determined.

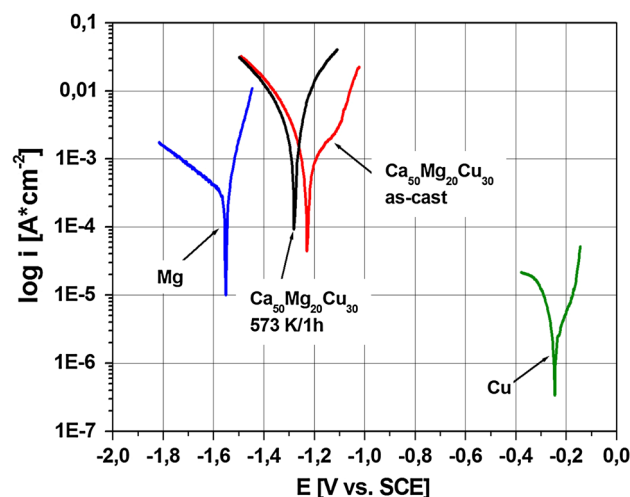


Fig. 6 The polarization curves recorded for the studied samples in a 5% NaCl solution at room temperature

The surface and fracture morphology of the $\text{Ca}_{50}\text{Mg}_{20}\text{Cu}_{30}$ master alloy was examined by SEM. The micrographs of the ingot-shaped sample show flat surface (Fig. 3a) and transcrystalline and brittle fracture (Fig. 3b). Melting and solidification curves of the studied master alloy are shown in Fig. 3(c). Based on the endothermic and exothermic features of the obtained DTA curves for the heating rate of 6 K/min, the onset of melting temperature (T_L) and the solidification point (T_S) were determined to be 622 and 677 K, respectively. Solidification of the liquid alloy showed a slight undercooling, as evidenced by the huge exothermic signal due to primary solidification.

Figure 4 presents the results of immersion tests for the studied glassy plates, performed in a 5% NaCl solution at room temperature in the time period from 10 to 70 min. The corrosion rate (V_{CORR}) after 10 min of immersion was equal to 0.024 mg/cm²/min and increased to 0.073 mg/cm²/min after 70 min for the “as-cast” sample. The change in corrosion rate of the same ternary $\text{Ca}_{50}\text{Mg}_{20}\text{Cu}_{30}$ glassy alloy in distilled water was also observed by Dahlam et al. The rapid decrease in weight, within time period from 150 to 500 h of immersion in water was observed. After 550 h of exposure, a rapid drop in the sample weight occurred leading to the complete decomposition of the sample (Ref 9).

The results obtained for the investigated alloy show that the volume of H_2 evolved after 70 min of immersion (2.87 mL/cm²) is very high in comparison with the measurements conducted by others (Ref 18). Approximately 2.3 mL/cm² of H_2 for pure Mg was obtained, where the exposition time of Mg specimens in a 3.5% NaCl solution was 14 days.

There is a linear relationship between the corrosion rate measured by the weight loss rate and that evaluated from the hydrogen evolution rate. The amount of evolved hydrogen and the corrosion rate increased with the increasing time of immersion. The line in Fig. 4 fits the obtained data well, and therefore, a linear character can be elucidated.

The results showing the open-circuit potential (E_{OCP}) variation with time recorded for the glassy, annealed alloy and the reference samples (Mg, Cu) are presented in Fig. 5. The E_{OCP} values of the two $\text{Ca}_{50}\text{Mg}_{20}\text{Cu}_{30}$ samples shift toward the positive potential fast in the initial 1000 s. The recorded E_{OCP} values of both $\text{Ca}_{50}\text{Mg}_{20}\text{Cu}_{30}$ alloy samples are higher than open-circuit potential of pure magnesium. This also indicates

Table 1 The results of the corrosion resistance investigations of the studied samples in a 5% NaCl solution (E_{OCP} —open-circuit potential, E_{CORR} —corrosion potential, β_a , β_c —anodic and cathodic Tafel slopes, R_p —polarization resistance, i_{CORR} —corrosion current density)

Sample	E_{OCP} , mV versus SCE	E_{CORR} , mV versus SCE	$ \beta_a $, mV	$ \beta_c $, mV	R_p , $\text{k}\Omega \text{ cm}^2$	i_{CORR} , $\mu\text{A}/\text{cm}^2$
Mg	−1645	−1648	68	419	0.029	883
Cu	−208	−220	449	200	4.695	13
Ca ₅₀ Mg ₂₀ Cu ₃₀ as-cast	−1253	−1248	165	79	0.011	2120
Ca ₅₀ Mg ₂₀ Cu ₃₀ 573 K/1 h	−1263	−1257	103	166	0.009	3110

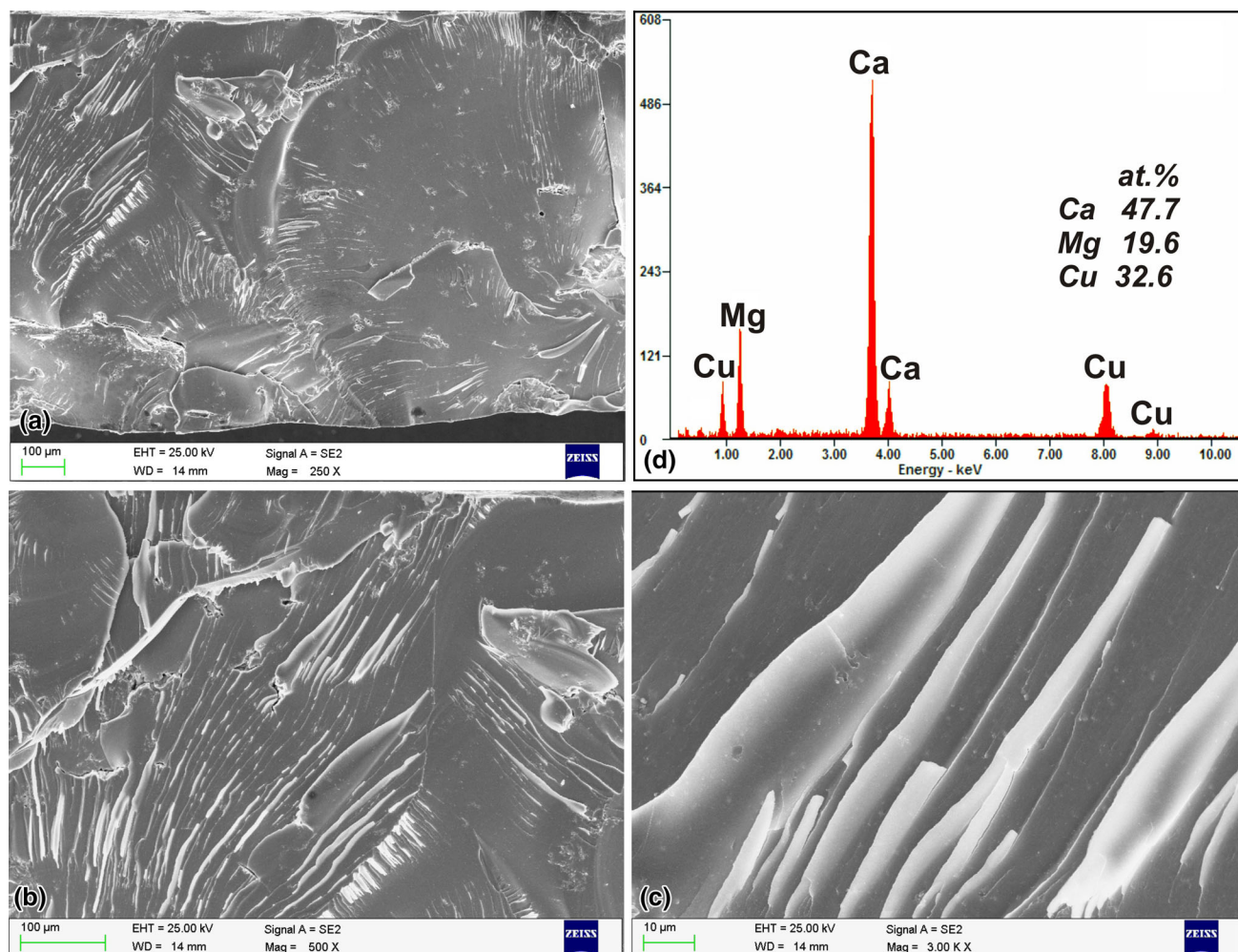


Fig. 7 SEM micrographs (a-c) and EDS analysis (d) of the fracture morphology of Ca₅₀Mg₂₀Cu₃₀ metallic glass in the as-cast state

higher corrosion resistance of the Ca₅₀Mg₂₀Cu₃₀ samples in comparison with Mg. Ca₅₀Mg₂₀Cu₃₀ glassy sample indicates a slightly more positive E_{OCP} value than that of sample after heat treatment, possibly attributed to the amorphous structure. The final value of the E_{OCP} for the glassy sample after 60 min of experiment was found to be equal to −1253 mV versus SCE. The highest E_{OCP} value was obtained for Cu specimen.

The typical potentiodynamic polarization curves recorded for pure Mg, Cu, and the alloy in the “as-cast” state and after annealing are presented in Fig. 6. The linear polarization method was applied for the calculation of the corrosion parameters and the results are summarized in Table 1. The

corrosion potential (E_{CORR}) of the pure Mg sample was −1648 mV versus SCE, corrosion current (i_{CORR}) density was 883 $\mu\text{A}/\text{cm}^2$, and the polarization resistance (R_p) was 0.029 $\text{k}\Omega \text{ cm}^2$. The “as-cast” Ca₅₀Mg₂₀Cu₃₀ alloy corrosion potential was equal to −1248 mV versus SCE, the corrosion current density increased to 2120 $\mu\text{A}/\text{cm}^2$, and the polarization resistance decreased to 0.011 $\text{k}\Omega \text{ cm}^2$. Cao et al. found that Ca-Mg-Zn bulk metallic glasses also possess larger noble corrosion potentials than crystalline high-purity Mg (E_{corr} = −1930 mV versus SCE). The E_{CORR} values of the six Ca-based amorphous alloys studied in Ref 21 varied from −1440 to −1390 mV versus SCE. In this study, the minimum essential medium

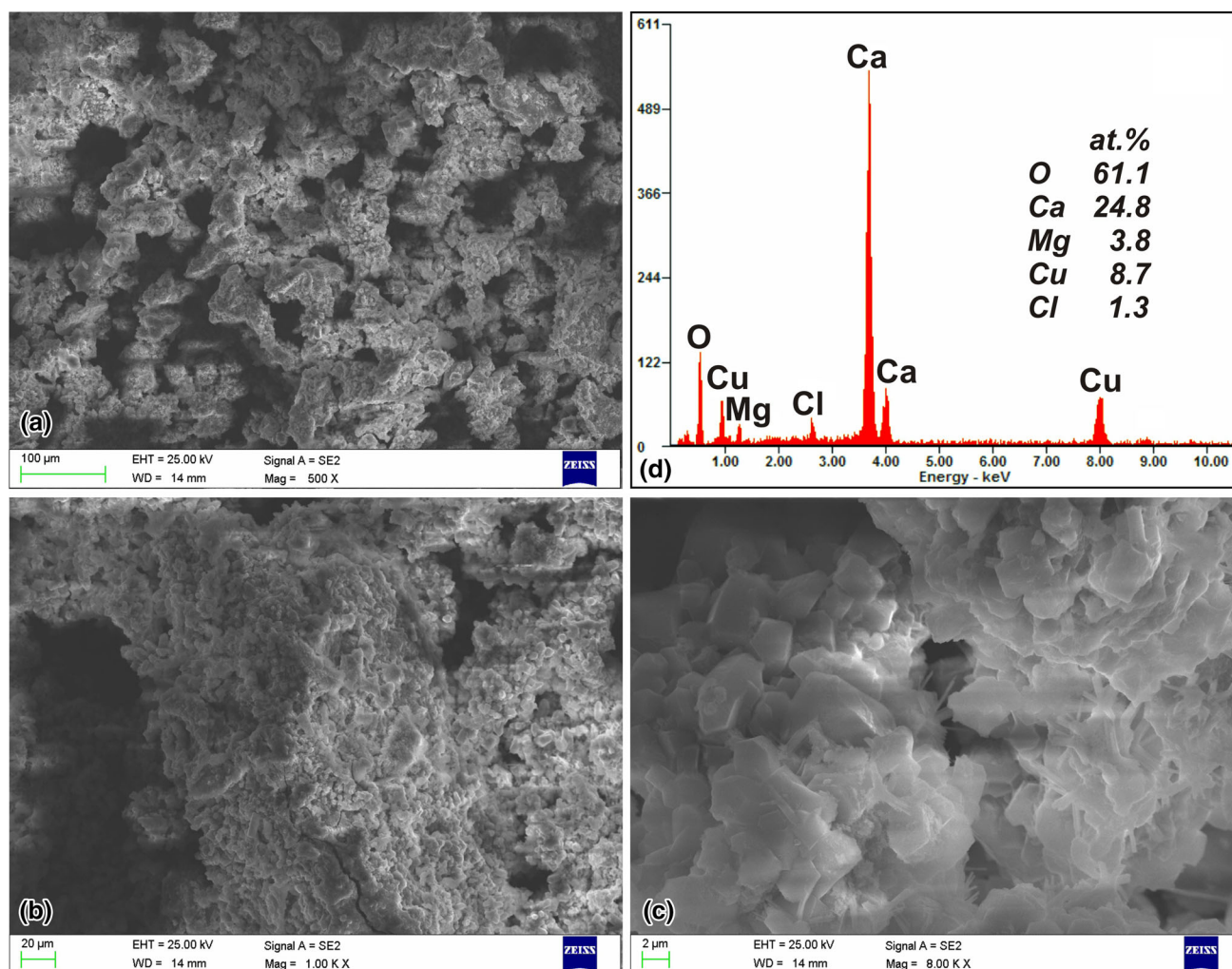


Fig. 8 SEM micrographs (a-c) and EDS analysis (d) of the surface morphology of $\text{Ca}_{50}\text{Mg}_{20}\text{Cu}_{30}$ metallic glass after corrosion tests

(MEM) was used as the electrolyte for the corrosion measurements. Moreover, the corrosion current density and corrosion potential of the Cu sample were lower than those of pure magnesium and the examined bulk amorphous Ca-based alloy.

The corrosion potential of the annealed alloy was found to be equal to -1257 mV versus SCE, while its corrosion current density was equal to $3110 \mu\text{A}/\text{cm}^2$. The polarization resistance determined for this sample was $0.009 \text{ k}\Omega \text{ cm}^2$. The heat treatment of the glassy sample resulted in a decrease in the corrosion potential and an increase in the corrosion current density. The E_{CORR} measured for the annealed sample was very close to the glassy one, but the i_{CORR} significantly decreased after the heat treatment. The worse corrosion resistance results of crystalline alloy should be referred to its multiphase structure (Mg_2Ca , CaCu , and Ca_2Cu phases identified after annealing, see Fig. 2b). Non-homogenous structure probably caused galvanic currents between crystalline phases and also influenced on inhomogeneous surface layer's growth.

Figure 7(a-c) shows the typical featureless mirror surface, which exhibits the “brittle” nature of Ca-based bulk metallic glasses. A great amount of parallel shear bands is clearly seen. The similar fracture morphology was reported by Liu et al. (Ref 22) for Mg-based bulk metallic glasses. This suggests the fracture of glassy alloy in the “as-cast” state occurs through a

typical brittle fracture mode described by Xu et al. (Ref 23). The brittle behavior of the examined material could be explained by the formation of complex glassy phase. According to the results of XRD analysis of the studied alloy in the “as-cast state” more complex amorphous structures consisting of at least two kinds of atomic clusters were formed simultaneously during rapid solidification process. The existence of different kinds of atomic clusters leads to the decrease in fracture strength. Moreover, EDS analysis shows that the composition of the master alloys is very close to the nominal (Fig. 7d). No presence of oxygen has been observed.

The surface morphologies of studied glassy alloy after corrosion tests in a 5% NaCl solution are shown in Fig. 8(a-c). The surface of the samples after tests remains flat and is still relatively whole, though some corrosion products have precipitated onto it. The EDS analysis demonstrated the presence of alloying elements Ca, Mg, Cu, and O on the sample's surface (Fig. 8d). Chlorine, also present on the surface, was a residual product from NaCl solution used for corrosion investigations. The EDS analysis results demonstrate that the ratio of Ca/O is 0.4. The presence of high oxygen concentration in the EDS spectrum probably suggests that oxides and hydroxides could be present on the surface of Ca-based metallic glasses after corrosion tests. The formation of a protective surface film (Ref

16, 24) could be also confirmed by the results of open-circuit potential measurements of the glassy sample.

Morrison et al. (Ref 8) also confirmed that $\text{Ca}_{55}\text{Mg}_{18}\text{Zn}_{11}\text{Cu}_{16}$ amorphous alloy after static aqueous immersion at room temperature exhibited corrosion resistance by forming protective film. These results indicate that the corrosion resistance of Ca-based bulk metallic glasses can be significantly improved by the addition of alloying elements such as Zn and Cu. Moreover, Inoue et al. (Ref 25) state that metallic glasses exhibit good corrosion resistance. The corrosion resistance of the homogeneous metallic glass is better than the crystalline materials or composites containing crystallites embedded in an amorphous matrix. Therefore, the corrosion behavior of amorphous alloys should be understood from the aspect of interaction of structure (lack of defects), chemical composition (passivating elements), and homogeneity (galvanic processes) (Ref 26).

4. Conclusions

The plates of Ca-based bulk metallic glass were successfully produced by pressure die casting. The diffraction pattern of the studied sample showed the broad diffraction halo indicating that the more complex amorphous structures consisting of at least two kinds of atomic clusters were formed simultaneously during the rapid solidification process. The XRD patterns of the samples after annealing at 573 K contain diffraction lines identified as corresponding to the crystalline hexagonal Mg_2Ca and orthorhombic CaCu , Ca_2Cu phases.

The alloy corrosion behavior was tested, and the corrosion rate was determined by immersion tests in a 5% NaCl solution. The alloy in the “as-cast” state displayed higher corrosion potential and better open-circuit potential than those of the tested alloy after the heat treatment and reference Mg sample. Corrosion resistance of $\text{Ca}_{50}\text{Mg}_{20}\text{Cu}_{30}$ alloy in the “as-cast” state was also characterized by hydrogen evolution during immersion test. The obtained results allow concluding that, there was a linear relationship of the amount of evolved hydrogen in a function of time.

The investigation of glassy alloy surface morphology after the corrosion tests showed the existence of oxide and hydroxide layers, which formed a good corrosion resistance barrier on the examined alloy. The presence of oxygen in the EDS spectra probably suggests that the mixture of Ca, Mg, and Cu oxides and hydroxides could be present on the surface of studied glassy samples after corrosion tests.

The Ca-Mg-Cu alloy studied in this work exhibits higher corrosion potential than that of the traditional magnesium in a 5% NaCl solution, which can open up an opportunity for the development of Ca-based alloy with potential applications.

Acknowledgments

The study was partially supported by the National Science Centre under research Project No.: 2011/03/D/ST8/04138.

Open Access

This article is distributed under the terms of the Creative Commons Attribution License which permits any use, distribution,

and reproduction in any medium, provided the original author(s) and the source are credited.

References

1. K. Amiya and A. Inoue, Formation and Thermal Stability of Ca-Mg-Ag-Cu Bulk Glassy Alloys, *Mater. Trans.*, 2002, **43**, p 81–84
2. O.N. Senkov, J.M. Scott, and D.B. Miracle, Composition Range and Glass Forming Ability of Ternary Ca-Mg-Cu Bulk Metallic Glasses, *J. Alloys Comp.*, 2006, **424**, p 394–399
3. O.N. Senkov and J.M. Scott, Formation and Thermal Stability of Ca-Mg-Zn and Ca-Mg-Zn-Cu Bulk Metallic Glasses, *Mater. Let.*, 2004, **58**, p 1375–1378
4. E.S. Park and D.H. Kim, Formation of Ca-Mg-Zn Bulk Glassy Alloy by Casting into Cone-Shaped Copper Mold, *J. Mater. Res.*, 2004, **19**, p 685–688
5. D. Okai, M. Inoue, T. Mori, T. Fukami, T. Yamasaki, H.M. Kimura, and A. Inoue, Annealing Effect on Mechanical Constants for $\text{Ca}_{48}\text{Mg}_{27}\text{Cu}_{25}$ Bulk Metallic Glass, *J. Alloys Compd.*, 2010, **504S**, p S95–S97
6. O.N. Senkov, D.B. Miracle, and J.M. Scott, Development and Characterization of Ca-Mg-Zn-Cu Bulk Metallic Glasses, *Intermetallics*, 2006, **14**, p 1055–1060
7. O.N. Senkov, J.M. Scott, and D.B. Miracle, Development of Low Density Ca-Mg-Al-Based Bulk Metallic Glasses, *Mater. Trans.*, 2007, **48**(7), p 1610–1616
8. M.L. Morrison, R.A. Buchanan, O.N. Senkov, D.B. Miracle, and P.K. Liaw, Electrochemical Behavior of Ca-Based Bulk Metallic Glasses, *Metall. Mater. Trans.*, 2006, **37**, p 1239–1245
9. J. Dahlman, O.N. Senkov, J.M. Scott, and D.B. Miracle, Corrosion Properties of Ca-Based Bulk Metallic Glasses, *Mater. Trans.*, 2007, **48**(7), p 1850–1854
10. R. Babilas, R. Nowosielski, W. Pilarczyk, and G. Dercz, Structural, Magnetic and Crystallization Study of Fe-Based Bulk Metallic Glasses, *Solid State Phenom.*, 2013, **203–204**, p 288–291
11. R. Babilas, K. Cesarz-Andraczke, R. Nowosielski, and A. Burian, Structure, Properties, and Crystallization of Mg-Cu-Y-Zn Bulk Metallic Glasses, *J. Mater. Eng. Perform.*, 2014, **23**(6), p 2241–2246
12. R. Nowosielski, R. Babilas, G. Dercz, and L. Pająk, Structure of Fe-Based Metallic Glass After Crystallization Process, *Solid State Phenom.*, 2010, **163**, p 165–168
13. S. Lesz, R. Babilas, and R. Nowosielski, Influence of Copper Addition on Glass Forming Ability, Thermal Stability, Structure and Magnetic Properties of Fe-Co-Based BMGs, *Solid State Phenom.*, 2013, **203–204**, p 296–301
14. H.P. Klug and L.E. Alexander, *X-ray Diffraction Procedures for Polycrystalline and Amorphous Materials*, Wiley, New York, 1962
15. A. Atrens, G.L. Song, F. Cao, Z. Shi, and P.K. Bowen, Advances in Mg Corrosion and Research Suggestions, *J. Magnes. Alloys*, 2013, **1**, p 177–200
16. A. Atrens, M. Liu, and N.I. Zainal Abidin, Corrosion Mechanism Applicable to Biodegradable Magnesium Implants, *Mater. Sci. Eng. B*, 2011, **176**, p 1609–1636
17. Z. Shi, M. Liu, and A. Atrens, Measurement of the Corrosion Rate of Magnesium Alloys Using Tafel Extrapolation, *Corros. Sci.*, 2010, **52**, p 579–588
18. Z. Shi and A. Atrens, An innovative Specimen Configuration for the Study of Mg Corrosion, *Corros. Sci.*, 2011, **53**, p 226–246
19. E.R. Barney, A.C. Hannon, O.N. Senkov, J.M. Scott, D.B. Miracle, and R.M. Moss, A Neutron and X-Ray Diffraction Study of Ca-Mg-Cu Metallic Glasses, *Intermetallics*, 2011, **19**, p 860–870
20. Powder Diffraction Files PDF-2, International Center for Diffraction Data
21. J.D. Cao, N.T. Kirkland, K.J. Laws, N. Biribilis, and M. Ferry, Ca-Mg-Zn Bulk Metallic Glasses as Bioresorbable Metals, *Acta Biomater.*, 2012, **8**, p 2375–2383
22. G. Liu, P. Gao, Z. Xue, Z. Tong, and M. Hang, Ultra-High Strength Mg-Li Based Bulk Metallic Glasses: Preparation and Performance Research, *Mater. Sci. Eng. A*, 2011, **528**, p 7156–7160

23. Y.K. Xu, H. Ma, J. Xu, and E. Ma, Mg-Based Bulk Metallic Glass Composites with Plasticity and Gigapascal Strength, *Acta Mater.*, 2005, **53**, p 1857–1866
24. W.W. He, E.L. Zhang, and K. Yang, Effect of Y on the Bio-Corrosion Behavior of Extruded Mg-Zn-Mn Alloy in Hank's Solution, *Mater. Sci. Eng. C*, 2010, **30**, p 167–174
25. A. Inoue and K. Hashimoto, *Amorphous and Nanocrystalline Materials: Preparation, Properties and Applications*, Springer, Berlin, 2001
26. A. Gebert, U. Wolff, A. John, and J. Eckert, Corrosion Behaviour of $\text{Mg}_{65}\text{Y}_{10}\text{Cu}_{25}$ Metallic Glass, *Scripta Mater.*, 2000, **43**, p 279–283